JOURNAL OF SOLID STATE CHEMISTRY 6, 213-221 (1973)

Structural Aspects of the Metal–Insulator Transitions in Ti_4O_7

M. MAREZIO, D. B. McWHAN, P. D. DERNIER, AND J. P. REMEIKA
Bell Laboratories, Murray Hill, New Jersey 07974

Received April 27, 1972

Ti_4O_7 has two transitions with decreasing temperature and the structure has been refined in each phase. The triclinic structure ($A\bar{1}$) consists of rutile-like layers of TiO_6 octahedra extending indefinitely in the *a–b* plane and four octahedra thick along the *c* axis. The average Ti–O distances for the four independent Ti atoms are 2.006(2), 2.006(2), 2.004(2), and 2.018(2) Å at 298K; 2.011(4), 2.000(4), 2.015(4), and 2.012(4) Å at 140K; 2.043(4), 1.973(4), 2.044(4), and 1.996(4) Å at 120K. At 120K there is a clear separation into strings of Ti^{3+} or Ti^{4+} ions running parallel to the pseudorutile *c* axis. In addition the 3+ sites are paired to form short Ti–Ti bonds, whereas the Ti^{4+} atoms are displaced toward one oxygen giving short Ti–O distances of 1.776(4) and 1.787(4) Å and thus forming a zig–zag chain. In the intermediate phase the interatomic distances are only slightly different from those at 298K but the thermal factors are anomalously large.

Introduction

Ti_4O_7 is a member of the homologous series Ti_nO_{2n-1} (*1–3*). Bartholomew and Frankl found a decrease of 10^5 in the electrical conductivity at two closely spaced temperatures, ~ 150 and ~ 125K (*4*). Mulay and Danley observed a drop of about a factor of 4 in the magnetic susceptibility at 150K (*5*). These authors measured the variation of the lattice parameters as a function of temperature and found a sharp increase in the unit-cell volume at ~ 150K (*6*). No discontinuities were observed in the lattice parameters at the lower transition. The extra reflections reported to appear at this transition (*4, 6*) were absent in a recently prepared, pure Ti_4O_7 powder sample.

The Ti_4O_7 structure consists of rutile-like slabs of TiO_6 octahedra extending indefinitely in two dimensions and four octahedra thick in the third dimension. The accurate determination of the structure (*7*) at room temperature revealed from the Ti–O distances that the effective ionic charge of all the titanium atoms is +3.5. This paper reports the accurate determination of the structure of the two phases stable in the range 150–125K and below 125K, respectively. The refinement of these two structures revealed that the unit cell previously chosen (*3, 7*) was actually *A* centered. For this reason and for comparative purposes we report again the room temperature structural data.

Crystal Data

Andersson and Jahnberg (*3*) were able to index on triclinic cells the powder patterns of each member of the homologous series, Ti_nO_{2n-1}, by recognizing in each pattern a rutile-like substructure. For Ti_4O_7 this cell turned out to be an *A*-centered cell.

Recently Horiuchi et al. (*8*) reported the crystallography of the isostructural series V_nO_{2n-1}. They proposed a primitive cell for every member of the series. In the case of Ti_4O_7 both cells, Andersson and Jahnberg's and Horiuchi et al.'s, give rise to an identical reduced cell. The matrix relating the two cells is:

Horiuchi et al. Andersson and Jahnberg

$$\begin{pmatrix} a \\ b \\ c \end{pmatrix}_T = \begin{pmatrix} 1 & 0 & 0 \\ 0 & 1 & 0 \\ 2 & \frac{5}{2} & \frac{1}{2} \end{pmatrix} \begin{pmatrix} a \\ b \\ c \end{pmatrix}_T$$

Since the *A*-centered cell proposed by Andersson and Jahnberg has interaxial angles closer to 90°, we found it convenient to describe the structure in this cell with an $A\bar{1}$ space group and 4 formula weights per unit cell.

In order to determine the lattice parameters and the unit cell in each phase of Ti_4O_7, powder data were obtained with a Philips Norelco Diffractometer fitted with an Air-Products and

Chemicals Cryotip device. In previous studies as a function of temperature two transitions were observed. At ~ 150K there were discontinuous changes in the lattice parameters and at ~ 125K extra reflections appeared. The powder samples were impure, however, and the extra reflections may have come from Ti_5O_9 which has a metal–insulator transition at ~ 130K. A single-phase sample of Ti_4O_7 was prepared using a previously prepared pure sample of Ti_3O_5. This latter compound was made by grinding together in an agate mortar the appropriate amounts of TiH_2 and TiO_2. The mixed powders were pressed at 5 tons in a $\frac{1}{4}$ in. die. The pellet was placed in a platinum boat which was then wrapped in a zirconium foil. The assembly was heated at 600°C in an argon atmosphere for 3 hr. Afterwards the temperature was raised to 1000°C and held for 24 hr. The Ti_3O_5 thus prepared was mixed with the appropriate amount of TiO_2 and the same procedure followed.

The Bragg angles of 21 well-resolved reflections were obtained at 298, 140 and 120K relative to those of a silicon internal standard. The lattice parameters determined by a least-squares refinement of the data are reported in Table I. They are in good agreement with the values obtained in the previous study. However, no extra reflections were observed below the 125K transition. The present powder X-ray data show no evidence for a doubling of the volume of the unit cell as was speculated from the previous data taken from impure samples. Long precession photographs were taken using single crystals for the room temperature structure determination. No extra reflections were observed in the low temperature phase. Each of the major axes of the crystal were scanned on the diffractometer, but no extra reflections were observed. There were discontinuous changes in the intensity of many reflections at both the 150 and 125K transitions. This

TABLE I

LATTICE PARAMETERS

	298K	140K	120K
a	5.593(1)	5.590(1)	5.591(1)
b	7.125(1)	7.128(1)	7.131(1)
c	12.456(3)	12.483(2)	12.487(2)
α	95.02(1)	95.03(1)	95.00(1)
β	95.21(1)	95.34(1)	95.33(1)
γ	108.73(1)	108.89(1)	108.88(1)

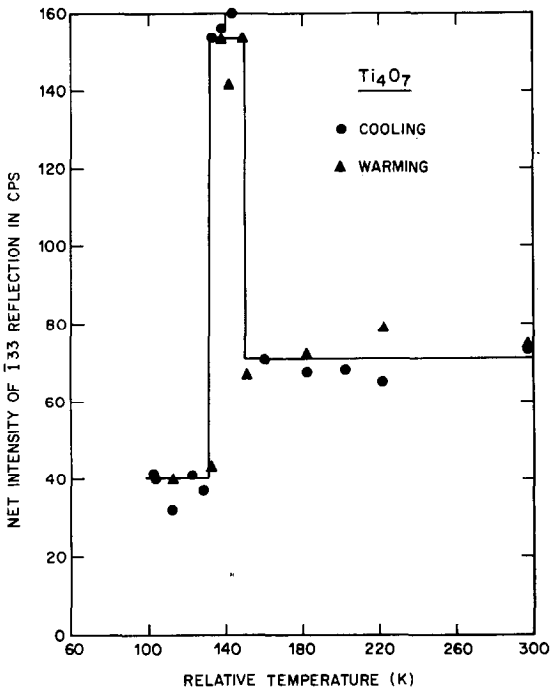

FIG. 1. The net intensity of the reflection (1̄33) in counts per second is shown versus temperature in degrees Kelvin. The temperatures are estimated from set points on the temperature controller, and therefore are relative only.

shows that the discontinuities in the conductivity are associated with first-order transitions in Ti_4O_7 and not due to possible Ti_5O_9 impurities as has been suggested (*9*). The intensity of the 1̄33 reflection as a function of temperature is shown in Fig. 1 to illustrate the X-ray evidence for both transitions. One concludes that both transitions are first order involving no change in symmetry but only rearrangements of the atoms within the unit cell.

Experimental

The intensity measurements were taken with a GEXRD-5 X-ray diffractometer. The machine settings and the specimen were the same as reported in Ref (*7*). Zr-filtered Mo$K\alpha$ radiation was used. The same reflections with $2\theta \leqslant 46°$ of observed magnitude at room temperature were collected at 140 and 120K. For each set of intensities the temperature was maintained by blowing a cold stream of nitrogen gas directly on the crystal. A Varian control unit was used to monitor and control the proper gas flow. The intensity of the reflection (1̄33) was a very sensitive

indicator of the range of stability of each of the respective phases as shown in Fig. 1. This reflection was used as a standard for the final set of data collection of the intermediate phase along with a strong reflection ($\bar{1}04$) as a check of sample orientation and ice buildup. The procedure for collecting intensities was the same for all phases. For each reflection, the approximate angles 2θ, χ, and ϕ were set automatically and then maximized by hand. The integrated intensities were obtained by use of the stationary crystal–stationary counter technique where the background was collected $\pm 2°$ 2θ off the peak maximum. The total number of reflections measured at 140 and 120K was 350 and the numbers observed were 331 and 335, respectively. The Lorentz, polarization, and absorption corrections were applied in order to convert the integrated intensities into structure factors. All Friedel pairs in the equatorial zone were also measured by hand at both temperatures and within experimental limits no differences between (hkl) and ($\bar{h}\bar{k}\bar{l}$) were observed. Most of these pairs had quite weak intensity and were therefore a sensitive indicator for the presence of the center of symmetry.

Refinement

In the refinement of the room temperature phase a pseudo-A-centered relationship was noted in the observed intensities. However, the refinement appeared to converge to a primitive cell. In refining the structure of the low temperature phase it became apparent that the true cell was A centered and that a false minimum had been reached in the earlier refinement at room temperature. Upon further least-squares refinement of the room temperature data the true minimum was reached with an A-centered cell which gave a lower set of standard deviations and conventional R and wR factors.

For each refinement the starting values for the positional and thermal parameters were the average A-centered related values at room temperature reported in Ref. (*7*). The f curves for neutral titanium and oxygen given by Cromer and Waber (*10*) were used along with the values of $\Delta f'$ and $\Delta f''$ reported by Cromer (*11*) in the least-squares refinement program ORFLS. Convergence was obtained after the first four cycles of refinement and anisotropic temperature factors were introduced during the last four cycles. The final positional parameters and the conventional R and wR factors are given in Table

TABLE II

FINAL POSITIONAL PARAMETERS

	298K	140K	120K
Ti(1)x	0.21617(8)	0.2173(2)	0.2367(2)
y	0.15282(7)	0.1560(2)	0.1634(2)
z	0.06282(3)	0.06404(9)	0.06824(9)
Ti(2)x	0.21852(8)	0.2172(2)	0.2129(2)
y	0.65258(7)	0.6549(2)	0.6714(2)
z	0.06618(3)	0.06596(9)	0.06558(9)
Ti(3)x	0.68340(7)	0.6816(2)	0.6693(2)
y	0.44002(6)	0.4424(2)	0.4389(2)
z	0.20115(3)	0.20048(9)	0.19376(9)
Ti(4)x	0.68858(7)	0.6875(2)	0.7057(2)
y	0.94231(6)	0.9425(2)	0.9492(2)
z	0.20136(3)	0.19988(9)	0.20440(8)
O(1)x	0.1073(3)	0.1077(7)	0.1080(7)
y	0.8627(3)	0.8618(6)	0.8616(6)
z	0.0151(1)	0.0156(3)	0.0165(3)
O(2)x	0.5870(3)	0.5871(8)	0.5803(7)
y	0.7922(3)	0.7925(6)	0.7967(6)
z	0.0577(1)	0.0567(3)	0.0618(3)
O(3)x	0.8558(3)	0.8538(7)	0.8573(7)
y	0.4964(3)	0.4967(6)	0.4961(6)
z	0.0811(1)	0.0800(3)	0.0742(3)
O(4)x	0.3281(3)	0.3233(7)	0.3159(7)
y	0.4385(3)	0.4400(6)	0.4455(6)
z	0.1387(1)	0.1395(3)	0.1423(3)
O(5)x	0.5265(3)	0.5280(7)	0.5283(6)
y	0.1449(3)	0.1425(6)	0.1362(6)
z	0.1639(1)	0.1659(3)	0.1691(3)
O(6)x	0.0377(3)	0.0388(7)	0.0373(7)
y	0.0700(3)	0.0691(6)	0.0706(6)
z	0.1981(1)	0.1972(3)	0.1980(3)
O(7)x	0.2946(3)	0.2925(7)	0.2849(7)
y	0.7905(3)	0.7854(6)	0.7794(6)
z	0.2238(1)	0.2234(3)	0.2224(3)
R factor	0.023	0.021	0.019
wR factor	0.039	0.030	0.029

TABLE III

FINAL THERMAL PARAMETERS ($\times 10^4$)

	298K	140K	120K
Ti(1)β_{11}	42(1)	61(5)	38(5)
β_{22}	24(1)	28(3)	17(3)
β_{33}	7.6(3)	6.4(8)	3.9(8)
β_{12}	10.2(8)	21(3)	19(2)
β_{13}	3.3(4)	7(1)	4(1)
β_{23}	1.7(4)	3(1)	0(1)
Ti(2)β_{11}	40(1)	54(5)	35(4)
β_{22}	23.0(9)	28(3)	15(3)
β_{33}	7.3(3)	5.7(8)	5.0(8)
β_{12}	10.2(8)	10(3)	13(3)
β_{13}	2.8(4)	3(1)	3(1)
β_{23}	1.4(3)	3(1)	−1(1)

TABLE III—(*continued*)

	298K	140K	120K
Ti(3)β_{11}	42(1)	54(5)	28(5)
β_{22}	21(1)	25(4)	16(3)
β_{33}	7.5(2)	10.1(9)	4.9(8)
β_{12}	9.1(7)	9(3)	9(3)
β_{13}	6.0(4)	9(1)	8(1)
β_{23}	2.1(3)	5(1)	3(1)
Ti(4)β_{11}	43(1)	59(5)	23(4)
β_{22}	25(1)	25(4)	18(3)
β_{33}	8.5(2)	6.9(8)	5.2(8)
β_{12}	11.5(8)	17(3)	12(2)
β_{13}	5.0(3)	1(1)	4(2)
β_{23}	2.3(3)	2(1)	2(1)
O(1)β_{11}	50(4)	50(12)	58(13)
β_{22}	32(3)	53(9)	20(9)
β_{33}	11(1)	16(3)	10(3)
β_{12}	14(3)	17(9)	14(9)
β_{13}	2(2)	6(5)	10(4)
β_{23}	3(1)	−2(4)	−4(4)
O(2)β_{11}	47(4)	76(13)	44(12)
β_{22}	34(3)	23(8)	17(8)
β_{33}	9.3(8)	15(2)	13(3)
β_{12}	8(3)	14(8)	20(8)
β_{13}	5(1)	−5(5)	9(5)
β_{23}	2(1)	2(3)	−3(4)
O(3)β_{11}	55(4)	51(13)	50(12)
β_{22}	39(3)	37(9)	35(9)
β_{33}	9.2(8)	16(2)	10(2)
β_{12}	11(3)	−2(9)	18(8)
β_{13}	10(2)	−1(5)	9(5)
β_{23}	3(1)	3(4)	−1(4)
O(4)β_{11}	53(4)	73(14)	70(13)
β_{22}	26(3)	39(8)	16(8)
β_{33}	7.6(8)	9(3)	6(2)
β_{12}	12(3)	1(8)	23(8)
β_{13}	2(2)	−5(5)	5(4)
β_{23}	0(1)	4(4)	−4(4)
O(5)β_{11}	47(4)	37(13)	62(13)
β_{22}	29(3)	52(9)	18(9)
β_{33}	9.4(9)	13(3)	6(3)
β_{12}	15(3)	5(9)	−2(9)
β_{13}	2(1)	−1(5)	6(5)
β_{23}	1(1)	6(4)	−3(4)
O(6)β_{11}	37(4)	76(14)	63(13)
β_{22}	36(3)	37(8)	39(9)
β_{33}	8.7(8)	12(3)	10(2)
β_{12}	11(3)	20(8)	18(9)
β_{13}	4(1)	4(5)	6(5)
β_{23}	2(1)	1(4)	2(4)
O(7)β_{11}	46(4)	58(13)	38(13)
β_{22}	30(3)	33(8)	34(9)
β_{33}	8.4(8)	10(3)	10(3)
β_{12}	14(3)	16(8)	7(9)
β_{13}	1(1)	−1(4)	9(4)
β_{23}	2(1)	−3(4)	8(4)

TABLE IV

INTERATOMIC DISTANCES (Å) IN Ti-OCTAHEDRA[a]

	298K	140K	120K
Ti(1)–O(1)	1.940(2)	1.949(4)	2.057(4)
–O(1)	1.977(2)	2.004(4)	2.058(4)
–O(2)	1.935(2)	1.936(4)	1.992(4)
–O(4)	2.041(2)	2.030(4)	2.030(4)
–O(5)	2.070(2)	2.088(4)	2.037(4)
–O(6)	2.071(2)	2.058(4)	2.086(4)
Average	2.006	2.011	2.043
O(5)–O(6) $e^{1/3}$	2.694(2)	2.686(6)	2.696(5)
O(5)–O(4) $e^{1/3}$	2.693(2)	2.745(6)	2.853(6)
O(5)–O(2)	2.883(3)	2.904(5)	3.002(5)
O(5)–O(1)	2.918(2)	2.919(5)	2.920(5)
O(1)–O(6)	2.834(3)	2.839(6)	2.854(5)
0(1)–0(4)	3.048(2)	3.038(5)	3.059(5)
O(1)–O(2)	2.896(3)	2.893(6)	2.952(6)
O(1)–O(1) $e^{1/1}$	2.639(4)	2.659(9)	2.667(8)
O(2)–O(4)	2.987(3)	3.009(6)	3.158(6)
O(2)–O(1)	2.786(2)	2.784(5)	2.813(5)
O(5)–O(4)	2.811(2)	2.804(6)	2.808(5)
O(5)–O(1)	2.734(3)	2.723(6)	2.733(6)
Ti(2)–O(1)	1.931(2)	1.902(4)	1.776(4)
–O(2)	1.997(2)	2.001(4)	1.964(4)
–O(3)	2.010(2)	2.011(4)	1.995(4)
–O(3)	1.976(2)	1.972(4)	1.958(4)
–O(4)	2.064(2)	2.068(5)	2.148(4)
–O(7)	2.061(2)	2.044(4)	1.995(4)
Average	2.006	2.000	1.973
O(7)–O(1)	2.866(2)	2.864(5)	2.845(5)
O(7)–O(2) $e^{2/4}$	2.749(2)	2.765(6)	2.700(5)
O(7)–O(3)	2.972(2)	2.953(5)	2.936(5)
O(7)–O(4) $e^{2/4}$	2.706(2)	2.654(6)	2.566(6)
O(3)–O(1)	2.806(3)	2.806(6)	2.772(6)
O(3)–O(2)	2.948(2)	2.924(5)	2.921(5)
O(3)–O(3) $e^{2/2}$	2.691(3)	2.691(8)	2.547(7)
O(3)–O(4)	2.965(2)	2.949(6)	2.897(5)
O(3)–O(1)	2.774(2)	2.760(5)	2.725(5)
O(3)–O(4)	2.841(2)	2.825(6)	2.770(6)
O(2)–O(1)	2.896(2)	2.887(6)	2.840(6)
O(2)–O(4)	2.798(2)	2.810(5)	2.791(5)
Ti(3)–O(5)	2.156(2)	2.146(4)	2.138(4)
–O(6)	1.935(2)	1.952(4)	2.049(4)
–O(7)	2.022(2)	2.039(4)	2.109(4)
O(5)	1.994(2)	2.018(4)	2.029(4)
O(4)	2.064(2)	2.070(4)	2.037(4)
O(3)	1.855(2)	1.862(4)	1.903(4)
Average	2.004	2.015	2.044
O(6)–O(5) $e^{3/1}$	2.694(2)	2.686(6)	2.696(5)
O(6)–O(7)	2.829(3)	2.845(7)	2.866(7)
O(6)–O(5)	2.911(2)	2.898(5)	2.896(5)
O(6)–O(3)	2.872(2)	2.900(5)	2.962(5)
O(4)–O(5) $f^{3/4}$	2.695(2)	2.670(5)	2.613(5)
O(4)–O(7) $f^{3/4}$	2.695(2)	2.716(5)	2.752(5)
O(4)–O(5) $e^{1/3}$	2.693(3)	2.745(6)	2.853(6)

TABLE IV—(*continued*)

	298K	140K	120K
O(4)–O(3)	3.008(2)	3.033(6)	3.138(6)
O(5)–O(7) $f^{3/4}$	2.649(2)	2.657(5)	2.644(5)
O(5)–O(5) $e^{3/3}$	2.601(3)	2.594(8)	2.588(7)
O(3)–O(7)	3.075(2)	3.103(6)	3.184(6)
O(3)–O(5)	2.926(2)	2.950(5)	3.042(5)
Ti(4)–O(4)	2.118(2)	2.117(4)	2.023(4)
–O(2)	1.939(2)	1.934(4)	1.945(4)
–O(7)	1.995(2)	1.985(4)	1.950(4)
–O(7)	2.176(2)	2.190(4)	2.314(4)
–O(6)	1.876(2)	1.882(4)	1.787(4)
–O(5)	2.001(2)	1.967(4)	1.958(4)
Average	2.018	2.012	1.996
O(4)–O(7) $e^{2/4}$	2.706(2)	2.654(6)	2.566(5)
O(4)–O(7) $f^{3/4}$	2.695(2)	2.716(5)	2.752(5)
O(4)–O(6)	3.001(2)	2.993(6)	2.918(5)
O(4)–O(5) $f^{3/4}$	2.695(2)	2.670(5)	2.613(5)
O(2)–O(7)	2.897(3)	2.909(5)	2.875(5)
O(2)–O(7) $e^{2/4}$	2.749(2)	2.765(6)	2.700(5)
O(2)–O(6)	2.954(2)	2.947(5)	2.936(5)
O(2)–O(5)	2.868(3)	2.866(7)	2.775(6)
O(7)–O(7) $e^{4/4}$	2.584(3)	2.571(8)	2.614(8)
O(7)–O(5) $f^{3/4}$	2.649(2)	2.657(5)	2.644(5)
O(6)–O(7)	2.948(2)	2.923(5)	2.884(5)
O(6)–O(5)	3.072(2)	3.062(6)	3.024(6)

[a] $e^{1/3}$ or $f^{5/8}$ next to an O–O distance indicate that the distance is either a shared edge or part of a shared face, between Ti(1)–Ti(3) and Ti(5)–Ti(8), respectively.

II. The final thermal parameters are reported in Table III. These values together with the lattice parameters reported in Table I were used as input to the program ORFFE which calculated the interatomic distances and thermal data reported in Tables IV–VII. The observed and calculated structure factors are available.[1]

Discussion

The new set of interatomic distances at room temperature are given in Table IV. The individual Ti(1)–O distances are the same as the average of those reported for the Ti(1)– and Ti(3)–octahedron in (7). In similar fashion the other pairs of *A*-centered related octahedra are Ti(2) and Ti(4), Ti(5) and Ti(7), and Ti(6) and Ti(8). The pairs of *A*-centered related oxygen atoms are O(1) and O(14), O(2) and O(13), O(3) and O(12), etc.

[1] A table of observed and calculated structure factors has been deposited as Document No. NAPS-01866 with the ASIS National Auxiliary Publications Service, C/O CCM Information Corp., 909 Third Avenue, New York, 10022. A copy may be secured by citing the document number. Advance payment is required. Make check or money order payable to ASIS-NAPS. (For current prices please check with NAPS.)

TABLE V

Ti–Ti Distances (Å)

	298K	140K	120K
Ti(1)–Ti(1)[a] edge	2.895(1)	2.926(2)	3.133(2)
–Ti(3)[a]	3.020(1)	2.990(2)	2.802(2)
–Ti(2)[a] corner	3.604(1)	3.609(1)	3.550(2)
–Ti(2)[a]	3.502(1)	3.491(1)	3.461(1)
–Ti(2)[a]	3.572(1)	3.574(3)	3.465(3)
–Ti(2)[a]	3.553(1)	3.554(3)	3.671(3)
–Ti(4)[a]	3.793(1)	3.783(2)	3.784(2)
–Ti(4)[a]	3.530(1)	3.526(2)	3.534(2)
–Ti(4)[a]	3.425(1)	3.434(2)	3.498(2)
–Ti(3)[b] edge	3.111(1)	3.124(2)	3.159(2)
–Ti(4)[b] corner	3.806(1)	3.795(2)	3.699(2)
Ti(2)–Ti(2)[a] edge	2.942(1)	2.937(2)	3.023(2)
–Ti(4)[a]	3.019(1)	3.000(2)	3.083(2)
–Ti(1)[a] corner	3.604(1)	3.609(1)	3.550(2)
–Ti(1)[a]	3.502(1)	3.481(1)	3.461(1)
–Ti(1)[a]	3.572(1)	3.574(3)	3.465(3)
–Ti(1)[a]	3.553(1)	3.554(3)	3.671(3)
–Ti(3)[a]	3.751(1)	3.746(2)	3.778(1)
–Ti(3)[a]	3.538(1)	3.539(2)	3.557(1)
–Ti(3)[a]	3.464(1)	3.473(2)	3.439(2)
–Ti(4)[b] edge	3.067(1)	3.101(2)	3.104(1)
–Ti(3)[b] corner	3.788(1)	3.773(2)	3.765(2)
Ti(3)–Ti(1)[a] edge	3.020(1)	2.990(2)	2.802(2)
–Ti(2)[a] corner	3.751(1)	3.746(2)	3.778(1)
–Ti(2)[a]	3.538(1)	3.539(2)	3.557(1)
–Ti(2)[a]	3.464(1)	3.473(2)	3.493(2)
–Ti(4)[a]	3.556(1)	3.573(2)	3.576(2)
–Ti(4)[a]	3.569(1)	3.555(2)	3.568(2)
–Ti(4)[b] face	2.811(1)	2.806(1)	2.838(1)
–Ti(4)[b] corner	3.417(1)	3.434(1)	3.414(1)
–Ti(3)[b] edge	3.237(1)	3.261(2)	3.267(1)
–Ti(1)[b]	3.111(1)	3.124(2)	3.159(2)
–Ti(2)[b] corner	3.788(1)	3.773(2)	3.765(2)
Ti(4)–Ti(2)[a] edge	3.019(1)	3.000(2)	3.083(2)
–Ti(1)[a] corner	3.793(1)	3.783(2)	3.784(2)
–Ti(1)[a]	3.530(1)	3.526(2)	3.534(2)
–Ti(1)[a]	3.425(1)	3.434(2)	3.498(2)
–Ti(3)[a]	3.556(1)	3.573(2)	3.576(2)
–Ti(3)[a]	3.569(1)	3.555(2)	3.568(2)
–Ti(3)[b] face	3.811(1)	2.806(1)	2.838(1)
–Ti(3)[b] corner	3.417(1)	3.434(1)	3.414(1)
–Ti(4)[b] edge	3.280(1)	3.295(2)	3.389(2)
–Ti(2)[b]	3.067(1)	3.101(1)	3.104(2)
–Ti(1)[b] corner	3.806(1)	3.795(2)	3.699(2)

[a] Distances inside the rutile blocks.

[b] Distances between rutile blocks.

TABLE VI

ROOT MEAN SQUARE VALUES

	298K	140K	120K
Ti(1) r_1	0.074(1)	0.063(5)	0.029(11)
r_2	0.074(1)	0.074(6)	0.061(6)
r_3	0.079(1)	0.095(4)	0.078(4)
Ti(2) r_1	0.072(1)	0.065(5)	0.042(8)
r_2	0.074(1)	0.080(5)	0.068(5)
r_3	0.076(1)	0.090(4)	0.072(4)
Ti(3) r_1	0.066(1)	0.066(5)	0.037(7)
r_2	0.070(1)	0.083(5)	0.058(6)
r_3	0.084(1)	0.098(4)	0.076(5)
Ti(4) r_1	0.072(1)	0.066(6)	0.046(7)
r_2	0.074(1)	0.074(5)	0.061(6)
r_3	0.084(1)	0.092(4)	0.069(5)
O(1) r_1	0.083(4)	0.081(11)	0.046(21)
r_2	0.085(4)	0.100(10)	0.083(11)
r_3	0.092(4)	0.124(10)	0.107(9)
O(2) r_1	0.076(4)	0.072(13)	0.023(36)
r_2	0.085(4)	0.091(11)	0.081(6)
r_3	0.095(4)	0.121(8)	0.107(10)
O(3) r_1	0.069(4)	0.073(12)	0.065(15)
r_2	0.093(4)	0.107(11)	0.089(10)
r_3	0.101(4)	0.118(9)	0.100(11)
O(4) r_1	0.073(4)	0.075(12)	0.024(39)
r_2	0.080(4)	0.086(11)	0.082(12)
r_3	0.087(4)	0.123(9)	0.099(9)
O(5) r_1	0.076(4)	0.070(14)	0.053(18)
r_2	0.082(4)	0.096(13)	0.070(15)
r_3	0.087(4)	0.119(9)	0.108(10)
O(6) r_1	0.070(4)	0.088(11)	0.084(12)
r_2	0.082(4)	0.098(11)	0.095(11)
r_3	0.093(4)	0.103(9)	0.096(10)
O(7) r_1	0.074(4)	0.074(12)	0.056(17)
r_2	0.083(4)	0.087(13)	0.087(12)
r_3	0.085(4)	0.102(11)	0.100(10)

TABLE VII

ROOT MEAN SQUARE COMPONENTS IN THE DIRECTION OF THE PSEUDORUTILE *c*-AXIS

	298K	140K	120K
Ti(1)	0.077	0.093	0.074
Ti(2)	0.075	0.080	0.067
Ti(3)	0.079	0.092	0.073
Ti(4)	0.081	0.085	0.067
Root mean square components in the direction of the pseudorutile (110)			
Ti(1)	0.076	0.071	0.063
Ti(2)	0.075	0.069	0.069
Ti(3)	0.072	0.075	0.053
Ti(4)	0.077	0.070	0.061
Root mean square components in the direction of Ti(3)–Ti(4) vector			
Ti(3)	0.069	0.81	0.045
Ti(4)	0.072	0.83	0.047

The structure of Ti_4O_7 consists of strings of edge-sharing octahedra running parallel to the pseudorutile *c* axis and truncated every four octahedra by the crystallographic shear planes, where the octahedra share faces. The pseudorutile blocks are bounded by these shear planes which run parallel to the *a–b* triclinic plane, as shown in Fig. 2. It should be pointed out that the crystallographic shear planes do not imply any shearing of one entire block with respect to the next. As in rutile, in every member of the homologous series Ti_nO_{2n-1} the oxygen array is hexagonal close-packed. At the crystallographic shear plane the titanium atoms fill the octahedral positions of the rutile cells at ($\frac{1}{2}$00) rather than filling the positions at (000). In Ti_4O_7 there are four crystallographically independent Ti atoms, two of which, Ti(1), Ti(2), are inside the blocks and two, Ti(3), Ti(4), at the end of the blocks. At room temperature the average Ti–O distances are Ti(1)–O = 2.006 Å; Ti(2)–O = 2.006 Å; Ti(3)–O = 2.004 Å; and Ti(4)–O = 2.018 Å, the overall average being 2.008 Å. By taking an average of the Shannon and Prewitt radii (*12*) for 3- and 4-coordinated O^{-2} and for 6-coordinated Ti^{3+} and Ti^{4+}, one obtains a calculated distance of 2.01 Å. One should note that the Ti(4)–O average distance is larger than the other three distances by approximately six times the standard deviation. The oxygen atoms are either 3- or 4-coordinated. O(1), O(2), and O(3), which are inside the rutile blocks are 3-coordinated. O(4), O(5), and O(7), which are shared between two blocks, are 4-coordinated. O(6) is 3-coordinated, but is shared between blocks. Inside the rutile blocks the shortest Ti–Ti distances are across the shared octahedral edges. In rutile TiO_2 (*13*) this distance is 2.958 Å, whereas in Ti_4O_7 it varies between 3.020 and 2.895 Å, the average being 2.986 Å. This larger average Ti–Ti distance is a consequence of the larger effective radius of $Ti^{3.5+}$. Octahedra between blocks share faces, edges, and corners. The shortest Ti–Ti distance between blocks, namely across the shared octahedral faces, is 2.811 Å. The Ti–Ti distances across the shared octahedral edges between blocks range from 3.067 to 3.280 Å. In Ti_2O_3 (*14*) the Ti–Ti distance across the shared octahedral face and across the shared octahedral edge are 2.592 and 2.990 Å, respectively.

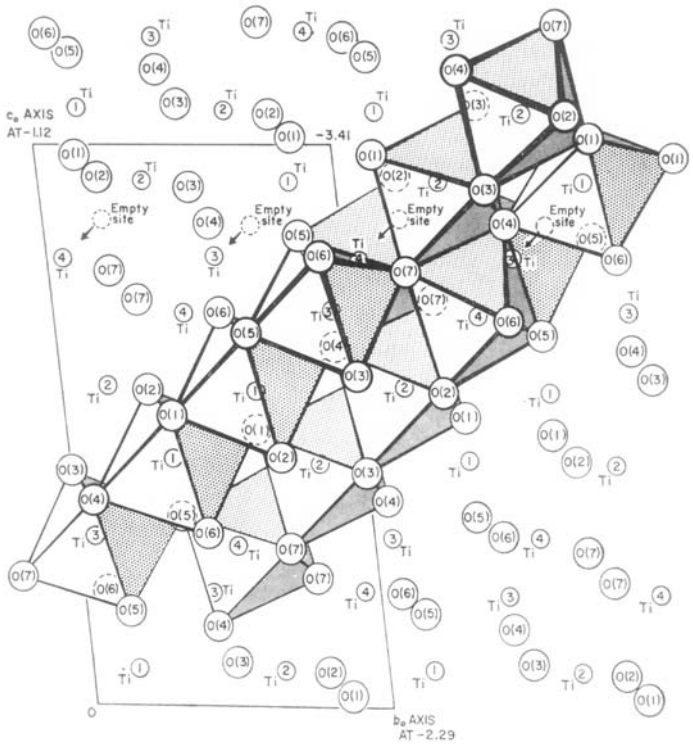

FIG. 2. A projection of the Ti_4O_7 structure looking down the triclinic *a* axis. The shaded set of octahedra runs roughly parallel to the pseudorutile *c* axis.

The final positional parameters of Ti_4O_7 at 140K, given in Table II, show that only small displacements occur at the 150K transition. The average of these displacements is approximately 0.015 Å. For the individual octahedra the average Ti–O distances are: Ti(1)–O = 2.011 Å; Ti(2)–O = 2.000 Å; Ti(3)–O = 2.015 Å; and Ti(4)–O = 2.012 Å. With respect to the equivalent distances at room temperature the Ti(1)– and Ti(3)–octahedra expand, whereas the Ti(2)– and Ti(4)–octahedra contract. It now appears that the Ti(2) sites accommodate more Ti^{4+} than the other three sites. The overall average Ti–O distance is 2.009 as compared to 2.008 Å at room temperature. In keeping with this increase the unit-cell volume expands ~ 0.4% at the 150K transition (*6*). All Ti–Ti distances across shared octahedral edges inside a rutile block decrease slightly, except the Ti(1)–Ti(1) distance which increases from 2.895 to 2.926 Å. The Ti–Ti distances across shared octahedral edges between rutile blocks increase, whereas the Ti(3)–Ti(4) distance across the shared octahedral face decreases from 2.811 to 2.806 Å.

As can be seen from Table II the positional parameters of the phase stable below the 125K transition are quite different from either the 298K phase or the 140K one. The displacements of the titanium atoms are about a factor of 10 larger than the displacements of the oxygen atoms. The displacements of the titanium atoms with respect to the 298K phase are about the same magnitude larger than the displacements of titanium atoms at the 150K transition. For the individual octahedra the average Ti–O distances are: Ti(1)–O = 2.043 Å; Ti(2)–O = 1.973; Ti(3)–O = 2.044 Å; and Ti(4)–O = 1.996 Å, the overall average being 2.014 Å. It is readily seen that in this phase the effective charge of Ti(1) and Ti(3) is 3+, whereas the effective charge of Ti(2) and Ti(4) is 4+. From the Shannon and Prewitt (*12*) ionic radii the calculated Ti–O distances are 2.04 and 1.98 for Ti^{3+} and Ti^{4+}, respectively. This is in excellent agreement with our experimental values. It is clear from Table IV that Ti(2) and Ti(4) have moved away from the center of the octahedron, along a perpendicular direction to the pseudorutile *c* axis, considerably more than Ti(1) and Ti(3). Consequently at 120K the Ti(1) and Ti(3) octahedra are less distorted than the Ti(2) and Ti(4) octahedra, whereas at 298 and

150K the Ti(1) and Ti(2) octahedra are less distorted. The Ti(1)–Ti(3) distance drops from 3.020 Å at 298K to 2.990 Å at 140K and to 2.802 Å at 120K. In contrast, all the other Ti–Ti distances across shared octahedral edges inside rutile blocks increase considerably. As can be seen from Fig. 3, the Ti(1), Ti(3) chains along the pseudorutile c axis consist of paired atoms with an effective charge of 3+, whereas the Ti(2), Ti(4) chains are unpaired and zigzag along the pseudorutile c axis. The zigzag arrangement is due to the displacements of the Ti(2) and Ti(4) atoms away from the octahedral centers along a direction perpendicular to the pseudorutile c axis. The Ti(3)–Ti(4) distance across the octahedral face decreases from 2.811 Å at 298K to 2.806 Å at 140K and increases to 2.838 Å at 120K. As mentioned previously the Ti(3) and Ti(4) atoms are not paired across the shared octahedral face at 298K and they have moved even further apart at 120K.

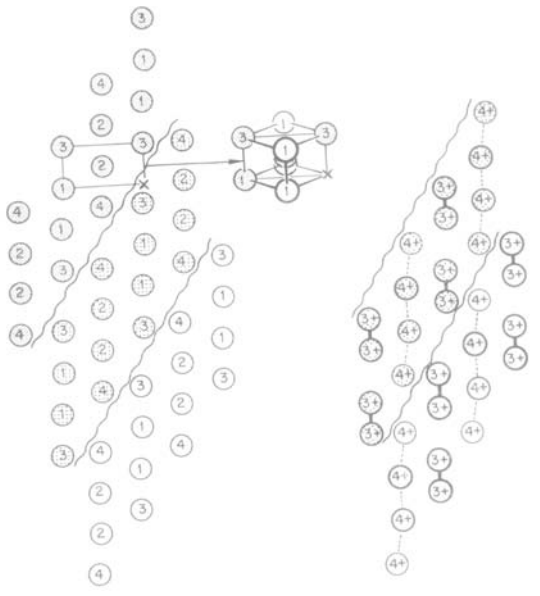

FIG. 3. At left are sheets of titanium ions in the Ti_4O_7 structure at 298K. The sheets of ions contain the pseudorutile directions [001] and [110] running vertically and horizontally, respectively. Each plane section is truncated by the shear planes as represented by the wavy lines while the various shadings indicate differences in the relative heights of each section. The shear planes intersect the plane of the paper at an angle of 64°. The outlined section is derived from the rutile cell shown in the center with the symbol "X" representing an empty site. The figure on the right represents equivalent sheets of titanium ions in the structure stable below 125K.

There are marked changes in the thermal parameters among the three phases with those of the 140K phase being anomalous (see Tables III, VI, and VII). At 298K the vibration of the titanium atoms inside the rutile blocks, Ti(1) and Ti(2), is nearly isotropic. The vibration of titanium atoms at the ends of the blocks, Ti(3) and Ti(4), is anisotropic with the smallest component directed toward the shared octahedral face. The largest component is directed toward the empty site resulting from the crystallographic shear plane. The thermal vibration of all the oxygen atoms is anisotropic. As one would expect the anistropy is larger for the 3-coordinated oxygen atoms than for the 4-coordinated ones. In contrast to the phase at 298K, the thermal vibrations of all the titanium atoms at 140K are anisotropic and anomalously large. Qualitatively this is true also for the oxygen atoms, but unfortunately for these atoms the standard deviations at 140K are too large to draw any unambiguous conclusion.

The magnitude of the ellipsoids are about the same for all four titaniums. One would expect the rms thermal displacements to decrease markedly with decreasing temperature, but in fact two of the principle axes of the thermal ellipsoids are larger at 140K than their counterparts at 298K. As can be seen from Tables VI and VII, the thermal ellipsoids of each titanium atom at 140K are oriented differently. For Ti(1) and Ti(3) the longest principle axis is along the pseudorutile c axis whereas for Ti(2) and Ti(4) the major axis makes an angle of about 25° with the pseudorutile c axis. At room temperature the smallest components of Ti(3) and Ti(4) are in the direction of the Ti(3)–Ti(4) vector which is normal to the shared octahedral face. At 140K this vector is no longer the minimum vibration even though the Ti(3)–Ti(4) distance has decreased slightly. The thermal ellipsoids decrease in magnitude on passing to the lowest temperature phase (125K). As in the intermediate phase the thermal vibration is anisotropic with the longest component along the pseudorutile c axis. The component along the Ti(3)–Ti(4) vector is the smallest as it was at room temperature.

Conclusions

The structural studies suggest the following model for the three phases. At room temperature Ti_4O_7 is a metal and an average valence of 3.5 is observed. At the lowest temperatures Ti_4O_7 is an

insulator and the magnetic susceptibility is low suggesting a nonmagnetic state. This is compatible with the separation of charge into Ti^{4+} sites containing no *d* electrons and Ti^{3+} sites in which the *d* electrons have paired to form a nonmagnetic bond as illustrated in Fig. 3. In the intermediate phase the resistivity has increased by 10^3 over the metallic phase and the magnetic susceptibility has dropped. There is no evidence for charge separation but the thermal factors are anomalously large. One can speculate that in the intermediate phase there is local charge separation and pair bonding but that there is no long-range order of the bonds. This would account for the large thermal vibrations in the bonding directions. The transition at $\sim$ 125K would then be viewed as the onset of long-range order of the pairing.

The structure of the phase at 120K is conceptually similar to that observed in $VO_2 + 2.4$ at % Cr. At the metal–insulator transition, half of the vanadium atoms pair along the pseudorutile *c* axis, while the other half zigzag along the same direction (*15*). The significant difference between the two is that there is evidence for charge separation only in Ti_4O_7 and not in $VO_2 + 2.4$ at % Cr. Also in the former the chains are broken by the crystallographic shear planes. Contrary to what has been speculated (*9*), no pairing of titanium atoms occurs across the shared octahedral faces, but instead the Ti(3)–Ti(4) interatomic distance actually increases from 2.811 Å at 298K to 2.836 at 120K. A similar increase from 2.697 to 2.746 Å occurs when proceeding from metallic V_2O_3 to insulating $V_2O_3 + 3.8$ at. % Cr (*16*). Both these compounds have the corundum structure and the arrangement between the blocks in Ti_4O_7 is also corundum-like.

The charge localization occurring in Ti_4O_7 is in a way similar to the scheme proposed by Verwey et al. (*17*) for the metal–insulator transition which occurs in Fe_3O_4 at 119K. The ordering scheme in the insulating phase has the Fe^{3+} and Fe^{2+} atoms occupying the octahedral sites, forming ordered mutually perpendicular rows. Neutron diffraction studies done by Hamilton (*18*) showed that this model is compatible with his experimental data. However, more recent electron microscopy work by Yamada et al. (*19*) and neutron scattering work by Samuelsen et al. (*20*) on magnetite proved that the unit cell of the low temperature phase is at least twice as large as that proposed by Verwey et al. Therefore, the ordering scheme must be more complicated than the one proposed by these authors. Thus the charge separation and pairing observed in Ti_4O_7 is probably the first clear example of a transition of the type envisioned by Verwey.

Acknowledgments

The authors wish to thank R. F. Bartholomew and W. B. White of the Materials Research Laboratory of Pennsylvania State University for kindly supplying the single crystals. We also like to thank T. M. Rice for many helpful discussions.

References

1. S. Andersson and A. Magnéli, *Naturwissenschaften* **43**, 495 (1956).
2. S. Andersson, B. Collin, U. Kuylensturna, and A. Magnéli, *Acta Chem. Scand.* **11**, 1461 (1957).
3. S. Andersson and L. Jahnberg, *Ark. Kem.* **21**, 413 (1963).
4. R. F. Bartholomew and D. R. Frankl, *Phys. Rev.* **187**, 828 (1969).
5. L. N. Mulay and W. J. Danley, *J. Appl. Phys.* **41**, 877 (1970).
6. M. Marezio, P. D. Dernier, D. B. McWhan, and J. P. Remeika, *Mater. Res. Bull.* **5**, 1015 (1970).
7. M. Marezio and P. D. Dernier, *J. Solid State Chem.* **3**, 340 (1971).
8. H. Horiuchi, M. Tokonami, N. Morimoto, K. Nagasawa, Y. Bando, and T. Takada, *Mater. Res. Bull.* **6**, 833 (1971).
9. J. B. Goodenough, *J. Solid State Chem.* **3**, 490 (1971).
10. D. T. Cromer and J. T. Waber, *Acta Crystallogr.* **18**, 104 (1965).
11. D. T. Cromer, *Acta Crystallogr.* **18**, 17 (1965).
12. R. D. Shannon and C. T. Prewitt, *Acta Crystallogr. Sect. B* **25**, 925 (1969).
13. S. C. Abrahams and J. L. Bernstein, *J. Chem. Phys.* **55**, 3206 (1971).
14. S. C. Abrahams, *Phys. Rev.* **130**, 2230 (1963).
15. M. Marezio, D. B. McWhan, J. P. Remeika, and P. D. Dernier, *Phys. Rev. B.* **5**, 2541 (1972),.
16. P. D. Dernier, *J. Phys. Chem. Solids* **31**, 2569 (1970).
17. E. J. Verwey, P. W. Haayman, and Romeijn, *J. Chem. Phys.* **15**, 181 (1947).
18. W. C. Hamilton, *Phys. Rev.* **110**, 1050 (1958).
19. T. Yamada, K. Suzuki, and S. Chikazumi, *Appl. Phys. Lett.* **13**, 172 (1968).
20. E. J. Samuelsen, E. J. Bleeker, L. Dobrzynski, and T. Riste, *J. Appl. Phys.* **39**, 1114 (1968).